Local strain-induced ferromagnetism in inhomogeneous Fe-implanted silicon carbide

A. Declémy, Lindor Diallo, Abdeslem Fnidiki, Luc Lechevallier, Jean Juraszek

Local strain-induced ferromagnetism in inhomogeneous Fe-implanted silicon carbide

A. Declémy[1], L. Diallo[2], A. Fnidiki[2], L. Lechevallier[2-3], J. Juraszek[2,*]

[1] UPR 3346 CNRS - Université de Poitiers – ENSMA - 11, Boulevard Marie et Pierre Curie – Site du Futuroscope – TSA 41123 – 86073 POITIERS CEDEX 9

[2] Normandie Univ., INSA Rouen, UNIROUEN, CNRS, GPM, 76800 Rouen, France.

[3]Département de GEII, Université de Cergy-Pontoise, rue d'Eragny, Neuville sur Oise, 95031 Cergy-Pontoise, France

*Corresponding author

Abstract

Despite an intense research on diluted magnetic semiconductors since twenty years ago, the origin and nature of observed ferromagnetism in these materials remain controversial, the presence of transition metal precipitates hindering to reveal unambiguously the intrinsic ferromagnetic behavior of the semiconducting matrix. In this work, we have investigated the magnetic properties of Fe-doped SiC, composed of Fe-rich nanoparticles and some diluted Fe atoms in the SiC matrix. By a careful analysis of the experimental magnetization data, a magnetic contribution from the diluted Fe atoms in the SiC matrix was evidenced, with a Curie temperature (T_C) value of ~115 K. Such a value is much higher than those reported in similar III-V diluted magnetic semiconductors such as a few at.% Mn-doped InP (T_C = 20-40 K). This magnetic ordering temperature of the diluted Fe atoms is shown to be independent of the amorphous or crystalline state of the SiC matrix, but depends strongly on the Fe-rich nanoparticle size, with a drastic reduction of T_C down to 45 K observed in the presence of Fe-rich nanoparticles with diameter higher than 10 nm.

Keywords: Diluted Magnetic Semiconductor (DMS), silicon carbide (SiC), Superconducting Quantum Interference Device magnetometry (SQUID), spin electronics.

Introduction

Light doping of semiconductors with a 3d magnetic element (Cr, Mn, Fe, Co) may confer ferromagnetic (FM) properties to the semiconductor material, leading to diluted magnetic semiconductors (DMS) able to be incorporated and operational in spintronic devices [1-2]. Since almost two decades, many advances have been made in the growth and annealing of these materials in order to minimize the presence of secondary phases or compensating defects which are detrimental to the desired properties with the goal to achieve Curie temperature (T_C) value higher than 300 K. Many authors have reported observation of ferromagnetism in such materials above room temperature (RT). However, most of these observations later turned out to be partial or full consequence of the presence of precipitates or inclusions of secondary phases of transition metal (TM) compounds in solid solution to which the DMS specimens belong [3-4]. These circumstances stimulated the appearance of theoretical works showing that the FM ordering in such specimens can be partly explained from the exchange interaction between charge carriers and doping magnetic ions [5-6]. Despite this intense research in DMS field, no T_C higher than RT has now been obtained and the origin and nature of observed ferromagnetism in these materials remain controversial [7]. Recently, a theoretical work [8] has addressed the nature of the ferromagnetism observed in 2.5-5 at.%Mn-doped InP [9] and another one [10] based on a self-consistent local random phase approximation (SC-LRPA) approach shed a new light on the complex topic of effects of magnetic inhomogeneities in DMS [11].

Among many candidates considered for spin electronics applications (III-V, II-VI compounds) the wide bandgap semiconductor silicon carbide (SiC) has a long history of materials research and device development and SiC-based components have already been commercialized for high frequency and high power applications. Many theoretical works [12-17] have shown that a magnetic moment may be attributed to TM atoms in different SiC polytypes and that electronic and magnetic properties of DMS are significantly influenced by the lattice relaxation [14-17]. Some authors [18] have claimed observation of ferromagnetism in Mn- and Fe-implanted 6H-SiC with T_C as high as 250 K. Typical FM order was also established at around 250 K at as low Mn-doped concentration as 10^{-4} molar fraction in 4H-SiC [19]. These authors found that defects-related effects other than the inserted Mn atoms play the most important role in the magnetic ordering. In addition, Liu et al experimentally evidenced ferromagnetism in 4H-SiC after neutron irradiation [20], suggesting that Si and C vacancies may also play an important role in magnetism in SiC. Despite this significant effort

to the theoretical and experimental investigations of TM-doped SiC and other DMS materials, the mechanisms responsible for the polarization and ordering in these materials are still far from being clear [7,15].

Ion implantation is now an essential industrial standard technique in doping semiconductors and can be usefull for obtaining high-spin configuration in SiC-based DMS [15]. In previously published works, some authors [21-24] have shown that the formation of Fe_3Si nanoparticles is mainly responsible for the magnetic properties observed in 6H-SiC crystals implanted with Fe ions at the 6 at.% concentration and annealed at high temperature (up to 1573 K). However, for Song *et al.* [25] the presence of Fe_3Si is not the nature origin of FM ordering in Fe-doped SiC, and traces of Fe-doping in SiC induce a high temperature FM arrangement. In recent communications [24,26,27], we reported atom probe tomography (APT) investigations on such materials, evidencing for a random distribution of Fe atoms in the SiC matrix and some Fe-rich nanoparticles. The FM behavior observed in hexagonal SiC implanted with 2-6 at.% Fe ions is mainly due to the contribution of Fe-rich nanoparticles, but also to an important part of diluted Fe atoms in the SiC matrix which can get a FM behavior [27-29].

The aim of the present work is to fully characterize the magnetic behavior of Fe-implanted SiC (Fe:SiC) with the two main populations of Fe atoms observed by APT in this system: Fe-rich noparticles and diluted Fe atoms in the SiC matrix. In the first part, experimental protocols are reported with relevant microstructural details of typical samples. Magnetometry results are presented with a complete treatment of the diamagnetic and paramagnetic contributions of the substrate to the measured signals. In many previously published works on this topic, this point is not well documented and/or taken account consideration, especially in TM-implanted samples in which the implanted thickness is much smaller (a few 100 nm) than the substrate one (a few 100 µm). When only correcting magnetization curves from the diamagnetic component of the substrate, the omission of the paramagnetic one may introduce a strong paramagnetic component in the temperature dependence of the net magnetization curves as we will show below. In the second and third parts, we present and discuss temperature dependence of the magnetization curves of typical samples. Modeling the Fe-rich nanoparticles contribution to the net magnetization of the studied samples allows to isolate the magnetic behavior of diluted Fe atoms and to compare it with the results of recent theoretical works [8,12,15]. It is shown that such a behavior as that observed in Fe-implanted SiC is common to other systems with similar electronic structure

like Mn-implanted InP [8], leading to a relatively high T_C ~ 115 K for FM diluted Fe atoms in SiC. At last, our results show an influence of big FM Fe-rich nanoparticles on the Curie temperature of the FM diluted Fe atoms.

I) Experimental

Lightly doped (a few 10^{+18} cm^{-3}) n- and p-type bulk 6H-SiC wafers (e ~ 350 µm) from CREE company have been implanted with Fe ions (^{56}Fe and also ^{57}Fe ions to enhance the statistics of the ^{57}Fe Mössbauer spectra). The implantation temperature was sufficiently high (653 K or 823 K) to prevent amorphization of SiC [30]. Each sample has been implanted with multiple energy Fe ions at different energies and fluences (from 30 to 160 keV at a few 10^{+15} to a few 10^{+16} Fe ions/cm²) in order to get a uniform Fe atom concentration $C_{at}Fe$ ~ 5.0 (+/-1.0)% from 20 to 90 nm under the sample surface. One sample was intentionally implanted at low temperature (473 K) and higher fluence in order to get an amorphous SiC matrix.

Post-implantation RTA (15 K/s) was performed at 1173 K, 1273 K or 1573 K with N_2 circulation in order to prevent accidental pollution. Actual Fe atom concentration profile and average value were measured by Rutheford Backscattering Spectroscopy (RBS) [31] and by EDS respectively.

The microstructural characterization of the as prepared samples was made by SEM and APT [32] to get a detailed picture of the Fe atoms distribution inside the SiC matrix. Finally, we used XRD to determine the surface normal strain profile along the **c**-axis of hexagonal SiC crystal within the implanted region [33-36] (See Supplementary Material for discussion).

The magnetic properties of the samples were studied by Superconducting QUantum Interference Device (SQUID), and ^{57}Fe conversion electron Mössbauer spectrometry (CEMS) which is sensitive to the near surface implanted region (~ 100 nm) [37,38]. The CEMS spectra were fitted with the Gunnlaugsson model [39] allowing to determine the proportion of implanted Fe atoms lying at substitutional position (noted Fe_S) into the SiC matrix. Previous works have shown that Fe atom more easily substitutes to Si rather than to C atom in SiC [13,16,40]. Thus, all along this work Fe_S denotes diluted Fe atoms at the Si sites in the SiC matrix. It could also be noted that there are crystallographic inequivalent Si (and C) sites when the first- and second-nearest neighbours are considered in 6H(4H)-SiC: two (6H-SiC) or one (4H-SiC) with cubic-like symmetry for one with hexagonal-like symmetry [41].

126

127 **I-1) Microstructural overview of some typical samples especially discussed in this work**

128

129 Table 1: Charateristics of the studied samples. *S*max is the maximum value of the surface
130 normal strain (see Supplementary Material); Fe-nanop is the proportion of Fe-implanted
131 atoms in the Fe-rich nanoparticles as obtained from APT and Fe_S is the proportion of Fe-
132 implanted atoms at the Si sites in the SiC matrix as obtained from CEMS as explained above.

SAMPLE	$C_{at}Fe$ (%)	T-implantation (K)	T-annealing (K)	Smax (%)	Fe-nanop (%)	Fe_S (%)
Sample 1	13	473	as-implanted	-	-	-
Sample 2	6	823	as-implanted	4	27	53
Sample 3	6	823	1173	3.5	44	43
Sample 4	4	823	1273	3.5	-	38
Sample 5	6	823	1573	3	66	24
Sample 6	2	823	1573	-	60	35

133

134 - The as-implanted sample at 473 K ($C_{at}Fe$ ~ 13%), under the SiC amorphization critical
135 temperature (~ 500 K) [30], shows an amorphous SiC matrix (RBS/Channeling and XRD)
136 and uniform contrast in SEM (no visible Fe-rich nanoparticles) (Sample 1; Fig.1-a).

137

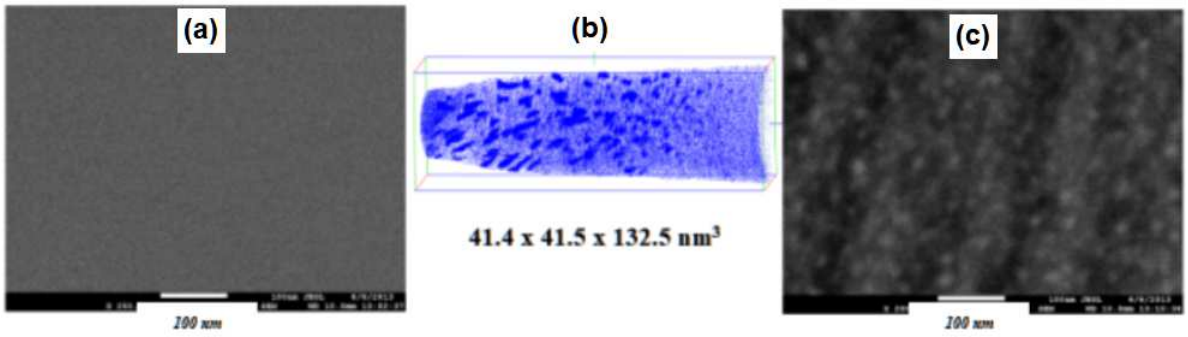

138

139 Fig. 1: **(a)**: Z-contrast image (SEM with BEI mode; backscattered electrons; HV = 20 kV) of sample 1;
140 **(b)**: APT image revealing Fe atoms spatial distribution in sample 3; **(c)**: Z-contrast image of sample 5

(the wave contrast is related to the p-type (> 10^{+19} cm^{-3}; Al doping) epitaxy (e ~ 200 nm) on n-type bulk substrate).

- The as-implanted sample at 823 K ($C_{at}Fe$ ~ 6%) shows a crystalline SiC matrix; slight contrasts are visible in SEM; small Fe-rich nanoparticles of mean diameter (diam) ~ 1-6 nm are detected by APT (core composition: $FeSi_2$; FeSi) [24,28] (Sample 2).

All the annealed samples at a given temperature (1173 K, 1273 K or 1573 K) with $C_{at}Fe$ ~ 5.0 (±1.0%) exhibit virtually similar microstructure independently of the implantation temperature (653 K or 823 K) and thus of their as-implanted state. It has been ensured that for more than 4 minutes RTA, there is no evolution of the microstructure and magnetic propreties. Thus, all RTA were done for a 4 minutes duration.

- The sample implanted at 823 K ($C_{at}Fe$ ~ 6%) and annealed at 1173 K shows a crystalline SiC matrix with a weak extra XRD peak (other than allowed 6H-SiC peaks; interreticular distance d ~ 0.2 nm and Scherrer diameter ~ 5 nm). Slight contrasts are visible in SEM; Fe-rich nanoparticles (diam ~ 1-8 nm) are detected by APT (core composition: FeSi; Fe_5Si_3; Fe_2Si) [24,28] (Sample 3; Fig. 1-b).

- The sample implanted at 653 K ($C_{at}Fe$ ~ 4%) and annealed at 1273 K shows a crystalline SiC matrix with an extra XRD peak (d ~ 0.2 nm and Scherrer diameter ~ 6 nm) and pockets on which a translation Moiré appears in TEM (d ~ 0.2 nm); slight contrasts are visible in SEM [23,28] (Sample 4).

- The sample implanted at 823 K ($C_{at}Fe$ ~ 6%) and annealed at 1573 K shows a crystalline SiC matrix with an extra XRD peak (d ~ 0.2 nm and Scherrer diameter > 6 nm) and pockets on which a translation Moiré appears in TEM (d ~ 0.2 nm). Clear contrasts are visible in SEM; Fe-rich nanoparticles (diam ~ 1-8 nm) and a few big (diam ~ 9-12 nm) Fe_3Si nanoparticles are detected by APT (core composition: FeSi; Fe_5Si_3; Fe_2Si; Fe_3Si) [24,28] (Sample 5; Fig.1-c).

- The sample implanted at 823 K ($C_{at}Fe$ ~ 2%) and annealed at 1573 K (Sample 6) with small (diam < 8 nm) superparamagnetic Fe-rich nanoparticles has been previously studied in [26,27,29].

I-2) Magnetometry

Magnetization loops M(H) were measured at 10 K and 250 K by SQUID with an applied field $\mu_o H$ varying from 0 to ± 2 T. As we can see on Fig. 2-a, the slope of SQUID signals at high field (> 0.3 T) is clearly different at 10 K and 250 K. For unimplanted and Fe-implanted samples, its value is ~ - 5.5 (A/m)/T at 10 K and ~ - 7.13 (A/m)/T at 250 K. Observation of the same slope for unimplanted and implanted samples shows no (or very weak) contribution of paramagnetic Fe-implanted atoms. Thus, this slope is mainly due to the diamagnetic component and to the paramagnetic defects of the bulk substrate 6H-SiC. These values lead to a slope ~ - 7.2 + 17 / T(K) [(A/m)/T] what is in the range of what is observed in the litterature for SiC. For example, the value of the calculated diamagnetic component for SiC is – 7.0 (A/m)/T [42] and the paramagnetic component corresponds to a concentration of paramagnetic defects ~ $2.7x10^{+18}$ cm^{-3} for $3.2x10^{+18}$ cm^{-3} observed by Wang [43] in lightly doped 6H-SiC from KMT company. Thus, all along this work we use the above value of the slope to properly eliminate the substrate contribution from the measured SQUID signals of the studied samples. Doing this for all the studied samples, saturation magnetization is observed and reached at $\mu_o H$ ~ 0.5 T at 10 K and 250 K, as shown on Fig. 2-b for sample 4.

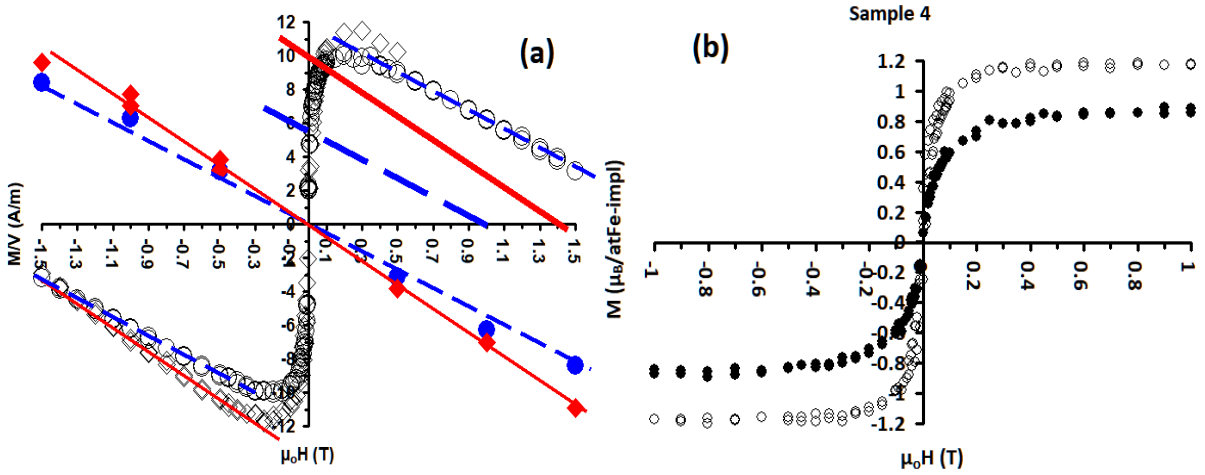

Fig. 2: **(a)**: SQUID magnetization curves of four SiC samples: unimplanted sample (full circles) and Fe-implanted sample (sample 1, empty circles) measured at 10 K: slope = - 5.5 (A/m)/T (dotted lines); unimplanted sample (full rhombus) and Fe-implanted sample (sample 5, empty rhombus) measured at 250 K: slope = - 7.13 (A/m)/T (continuous lines). **(b)**: Magnetic moment of sample 4 as a function of

193 the applied field $\mu_o H$ in Tesla (T): measured at T = 10 K (empty circles) and T = 250 K (full circles).
194 The value of the magnetic moment is given in μ_B per Fe-implanted atom (μ_B/at-Fe impl) where μ_B is
195 the Bohr magneton.

196

197 Open cycles are observed at 10 K (Fig. 3). At 250 K the cycles are closed or under
198 resolution, except for sample 5. For sample 1 (Fig. 3-a) with no Fe-rich nanoparticle, the FM
199 behavior at 10 K is clearly evidenced.

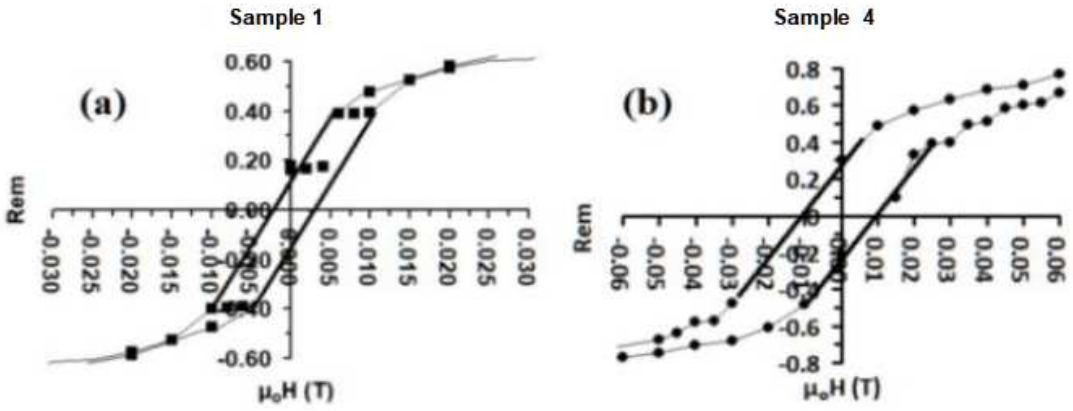

200

201 Fig. 3: FM loops at 10 K. **(a)**: Sample 1: Magnetization remanence (*Rem*) ~ 10% and coercive field
202 (H_C) ~ 2.5 mT; **(b)**: Sample 4: *Rem* ~ 25% and H_C ~ 10 mT.

203

204 For the other samples containing Fe-rich nanoparticles, this demonstrates the FM
205 behavior at 10 K and the superparamagnetic behavior at 250 K, what is confirmed by FC/ZFC
206 curves at low field as shown on Fig. 4 with a blocking temperature T_B ~ 45 K for sample 4
207 (Fig. 4-a).

208

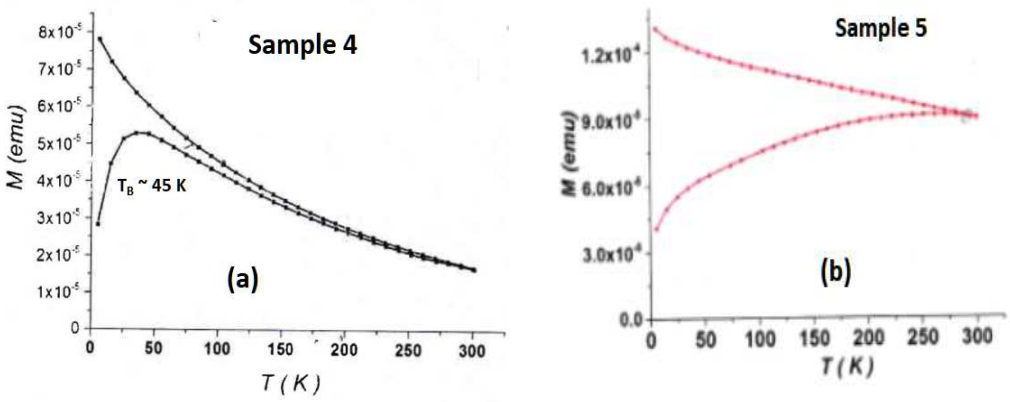

Fig. 4: FC/ZFC curves at low field ($\mu_o H = 0.01$ T). **(a)**: Sample 4; **(b)**: Sample 5.

For sample 5 with big (diam ~ 9-12 nm) Fe_3Si nanoparticles, the ZFC curve shows no maximum and magnetization increases continuously with increasing temperature (Fig. 4-b). This shows the FM character of this sample as for a solid sample with T_B > 300 K. Indeed, a slight open cycle is observed at 250 K (*Rem* ~ 10% with a H_C ~ 5 mT) and CEMS at 300 K shows a clear signature of a FM Fe_3Si component [28].

Due to the complex Stoner-Wohlfarth behavior of the superparamagnetic Fe-rich nanoparticles at low temperature and low field, remanent magnetization could be difficult to interpret for samples containing Fe-rich nanoparticles due to the mixing of their FM behavior for T < T_B with that of diluted Fe atoms as shown in Fig. 3-a for sample 1 with no Fe-rich nanoparticle. Thus, in order to properly quantify the magnetic behavior of the different Fe phases observed in the studied samples (Fe-rich nanoparticles and diluted Fe atoms in the SiC matrix) magnetization curves as a function of temperature M(T) have been measured at saturation with an applied field $\mu_o H = 0.5$ T from 10 K to 250 K.

II) Results and discussion

As shown on Fig. 5-a, the M(T) curve of sample 1 (with no Fe-rich nanoparticle) reaches ~ 0 at high temperature with a "highly unconventional non-Brillouin-function-like character" [8]. In other samples with Fe-rich nanoparticles M(T) is smoother and higher, revealing the magnetization of superparamagnetic Fe-rich nanoparticles with a $T_C \geq 350$ K.

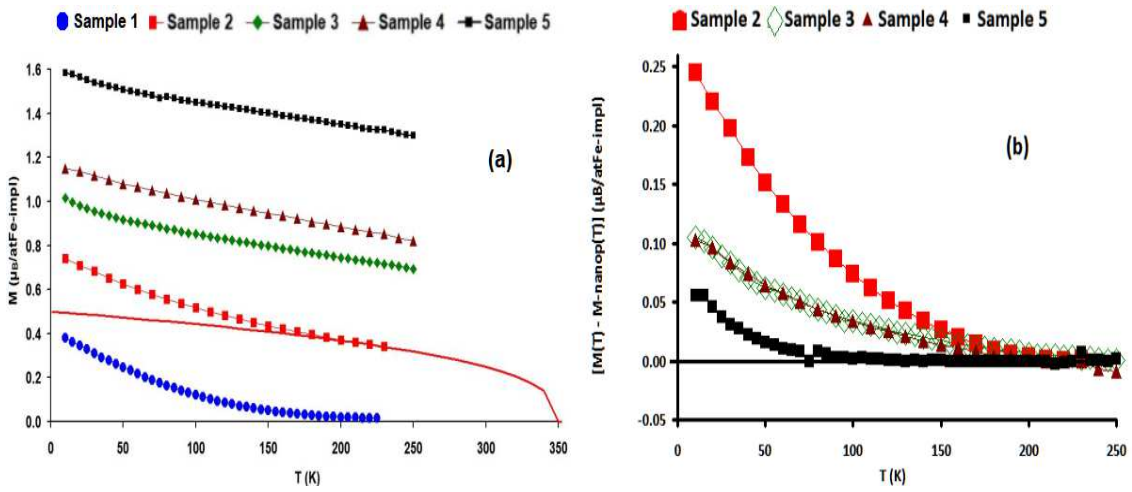

229

230 Fig. 5: **(a)**: Saturation magnetization of samples 1-5 as a function of temperature. Line: Brillouin-
231 function-like magnetization of Fe-rich nanoparticles for sample 2 calculated from equation (1) with
232 M(0)-nanop = 0.5 μ_B/atFe-impl and T_C-nanop = 350 K (see later and Table 2). **(b)**: [M(T) – M-
233 nanop(T)] for samples 2 to 5.

234 In order to identify the contribution of the Fe-rich nanoparticles and the contribution
235 of the diluted Fe atoms in the SiC matrix to the net magnetization, it is possible to describe the
236 temperature dependence of the saturation magnetization of the superparamagnetic Fe-rich
237 nanoparticles by the following relation:

238 $$\text{M-nanop(T)} = \text{M(0)-nanop}\ (1 - T/T_C\text{-nanop})^{\beta} \qquad (1)$$

239 where M(0)-nanop is the value of their saturation magnetization at T = 0 K, T_C-nanop is their
240 Curie temperature, and β is the critical exponent with β = 0.36 for Heisenberg ferromagnets
241 [44-45]. As previously noted in [29], equation (1) is unable to reproduce the full behavior of
242 M(T) curves namely at low temperature as shown in Fig.5 for sample 2. Then, fitting the
243 maximum number of points of high temperature part of all these curves with equation (1)
244 leads to the values of M(0)-nanop and T_C-nanop reported in Table 2.

245

246 Table 2: M(0)-nanop and T_C-nanop are relative to Fe-rich nanoparticles. M(0)-diluted and T_C-diluted
247 are relative to diluted Fe atoms in the SiC matrix and were obtained as explained in the text below.
248 The values of M(0)-nanop and M(0)-diluted are in μ_B/atFe-impl.

SAMPLE	M(0)-nanop	T_C-nanop (K)	M(0)-diluted	T_C-diluted (K)
Sample 1	-	-	0.40	110

Sample 2	0.5	350	0.275	110
Sample 3	0.89	500	0.10	110
Sample 4	1.055	515	0.11	120
Sample 5	1.535	700	0.07	45
Sample 6	1.285	615	0.14	120

Substracting this contribution from the M(T) curves for samples 2 to 6, a residual contribution appears which can be identify with the contribution of the diluted Fe atoms in the SiC matrix (M(T)-diluted). All these M(T)-diluted = M(T) - M-nanop(T) curves (Fig. 5-b) exhibit the same behavior as the M(T) curve of sample 1 (Fig. 5-a) showing that diluted Fe atoms of these samples with nanoparticles have the same magnetic behavior as Fe atoms in sample 1 with no nanoparticle.

II-1) Theoretical analysis

Los et *al* [15] theoretically studied purely diluted 4 at.%Fe-doped hexagonal SiC (with no nanoparticules or other kind of defects) with *ab initio* calculations taking "fully account for the effects of crystal lattice reconstruction and electronic structure changes caused by substitution of Si atoms by Fe atoms". They show that "substitution of 4% of Si atoms in the SiC lattice with Fe atoms leads to an emergence of two impurity bands in the gap close to the valence band top. The Fermi level is then pinned in the middle of the lower-energy Fe band with close to 100% spin polarization" together with a lattice relaxation along the **c**-axis of the hexagonal SiC crytal. Fe atom being at a hexagonal-like Si site, the C atom above the Fe atom among the four C atoms forming the elemental tetrahedra around Fe atom have the strongest influence on the electronic and magnetic configurations. While with Fe atom at a cubic-like Si site there is no atomic relaxation for the non magnetic state (NM), in the high spin magnetic state (M), the equilibrium distance between Fe atom and C atom above it in the tetrahedron is significantly increased. Fe atom is staying practically in place and this C atom is moving about 0.01 nm away along the **c**-axis of the hexagonal SiC crytal from the unrelaxed Fe-C distance of ~ 0.19 nm (= Si-C distance in SiC) for a strain value of ~ 5%. The NM state becomes the lower energy state for a strain less than 2.5% as shown on Fig. 3 of [15]. In the

M state, such value of strain corresponds to the surface normal strain measured by XRD along the **c**-axis of the hexagonal SiC crystal (3-4%; see Table 1 and Supplementary Material).

On the other hand, in a recent theoretical work on the origin of ferromagnetism in III-V DMS, , Bouzerar et *al* [8] combine several theoretical approaches to explain the magnetic properties of such systems, and in particular on 2.5-5 at.%Mn-implanted InP [9]. It is shown that the "highly unconventional non-Brillouin-function-like character" of the M(T) curve for this system is strongly related to "the extreme sensitivity of the position of the Mn acceptor level". Moreover, "spin-resolved density of states (DOS) in (In,Mn)P itinerant carriers are always fully polarized and the Fermi level lies in a well defined impurity band not totally separated from the valence band" [8]. The electronic structure of 2.5-5 at.%Mn-implanted InP and of 4 at.%Fe-doped hexagonal SiC are thus very similar, allowing analysis of our experimental results in the framework of Refs [8] and [15].

For comparison, the ordinate axis of calculated curves of [8] were normalized to that of the experimental ones of [9]. As shown in Fig. 6-a the value T_C ~ 40 K for 5 at.%Mn-implanted InP reported in [9] and calculated in [8] corresponds to about the quarter of the maximum value of the experimental M(T) curves and of the normalized calculated ones at low temperature (large arrows on Fig. 6-a).

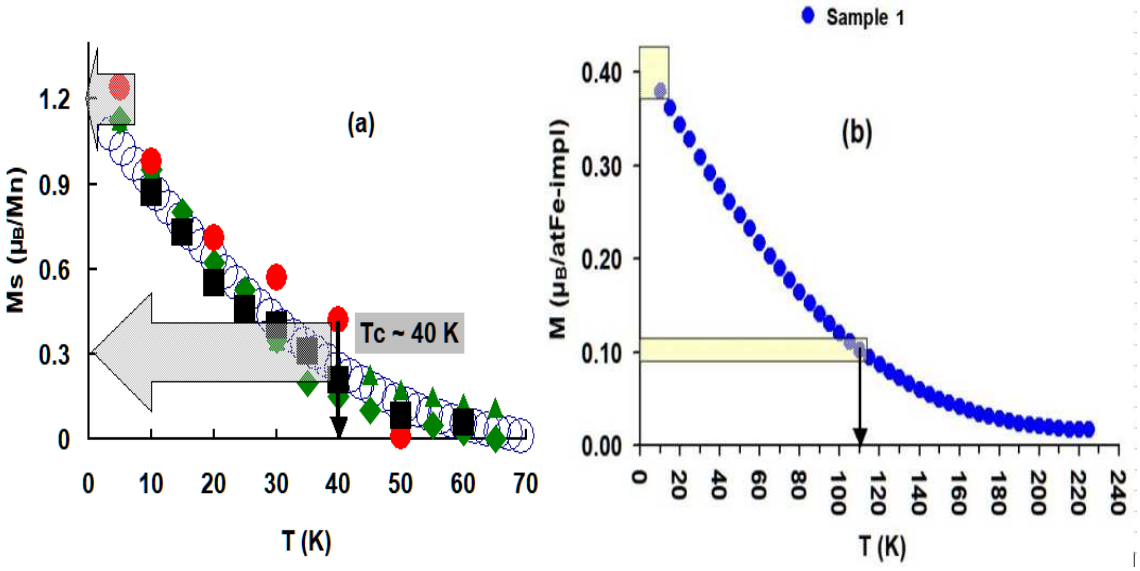

Fig. 6: **(a)**: 5 at.%Mn-implanted InP saturation magnetization Ms(μ_B/Mn) as a function of temperature: SQUID (full circles) and XMCD signal (squares) [9]; normalized calculations MC (triangles) and LRPA (rhombus) [8]; normalized M(T) curve of sample 1 (empty circles). **(b)**: experimental saturation magnetization M(T) curve of sample 1.

With this criterion, we can evaluate the value T_C ~ 110 K for sample 1 (Fig. 6-b). Normalizing the experimental M(T) curve of sample 1 with: Mx1.2/0.4 and Tx40/110, we can see that the normalized curve of this sample exactly overlaps the experimental curves of 5 at.%Mn-implanted InP and the normalized calculated ones (Fig. 6-a). This confirms that (In,Mn)P and Fe:SiC have similar electronic structure and magnetic behavior. We conclude that sample 1 has a DMS behavior with T_C ~ 110 K.

The M(T)-diluted curves for samples with nanoparticles (Fig. 5-b) can then be analyzed as explained above for sample 1. Thus, normalizing these curves with Mx1.2/M(0)-diluted and Tx40/T_C-diluted with the set of parameters given in Table 2, as we have done above for sample 1, all the normalized curves remarkably overlap the normalized curve of sample 1 as shown in Fig. 7. This shows that the magnetic behavior of diluted Fe atoms in Fe:SiC can be described and explained, as for the III-V system (In,Mn)P, in the framework of the theoretical work of [8], independently of the presence of Fe-rich nanoparticles. We are thus able to evaluate the mean value of the magnetic moment of the diluted Fe atoms (M(0)-diluted) and their Curie temperature (T_C-diluted) as reported in Table 2.

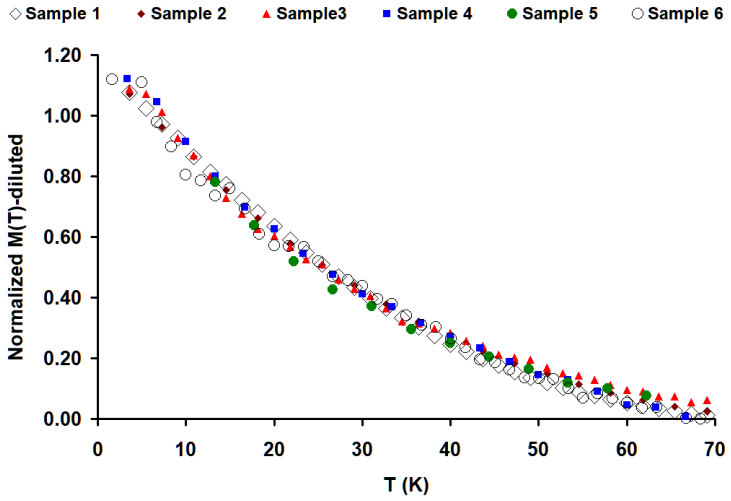

Fig. 7: Normalized M(T)-diluted curves as explained in the text.

Only the diamagnetic component of the substrate has been taken into account in previous work [29] and then, as mentioned above, a strong paramagnetic component appears on the M(T) curve of sample 6. In the present work, subtracting the paramagnetic contribution of the substrate from magnetometry measurements leads to the normalized M(T)-diluted curve of Fig. 7 together with the set of parameters reported in Table 2 for this sample.

315

316 **II-2) Discussion on Curie Temperature**

317 The values of T_C-nanop reported on Table 2 are in the range of the FM compounds present in
318 the Fe-rich nanoparticles evidenced by APT in the studied samples [24,27]: $T_C(Fe_5Si)$ ~ 385
319 K; $T_C(Fe_2Si)$ ~ 550 K; $T_C(Fe_3Si)$ ~ 840 K. The mean value of T_C-diluted is ~ 115(+/-5) K in
320 all samples independently of the amorphous or crystalline state of the SiC matrix and of the
321 presence of small (diam < 10 nm) superparamagnetic Fe-rich nanoparticles, except for sample
322 5 with a few big (diam ~ 9-12 nm) strongly FM Fe_3Si nanoparticles. In that case, T_C-diluted is
323 strongly reduced to 45 K, indicating a strong influence of strongly FM big Fe_3Si nanoparticles
324 on the FM behavior of diluted Fe atoms. It can be mentioned that the sample 6 ($C_{at}Fe$ ~ 2%)
325 annealed at the same temperature (1573 K) as sample 5 ($C_{at}Fe$ ~ 6%) exhibits only small
326 (diam < 8 nm) superparamagnetic Fe-rich nanoparticles [27] and T_C-diluted ~ 120 K (Table
327 2), confirming the strong influence of strongly FM big Fe-rich nanoparticles on the magnetic
328 behavior of diluted Fe atoms in Fe:SiC.

329 **II-3) Discussion on TM magnetic moment**

330 The mean value of the magnetic moment of Fe atoms in Fe-rich nanoparticules can be
331 evaluated as: M(0)-Fe-nanop = M0)-nanop / Fe-nanop as reported in Table 3 where results
332 obtained from other techniques are also given (Fe-nanop ans Fe_S, see Table 1). The median
333 value of M(0)-Fe-nanop on the five samples containing nanoparticles (samples 2 to 6) is ~ 2.1
334 μ_B, as currently observed for Fe atoms in the high spin state in well defined solid FM
335 compounds mainly detected by APT in the core of the Fe-rich nanoparticles. In a previous
336 work [27], we have estimated *a priori* the mean value of the magnetic moment of Fe atoms in
337 Fe-rich nanoparticles from its mean value in these solid FM compounds. The value of the
338 magnetic moment (~ 1.2 μ_B) [27] appears now to be underestimated and therefore
339 overestimated values of the magnetic moment of diluted Fe atoms were obtained. In the
340 present work, modeling the contribution of the Fe-rich nanoparticles to the saturation
341 magnetization with equation (1) and taking into account the proportion of Fe-implanted atoms
342 in the Fe-rich nanoparticles obtained from APT (Fe-nanop) get a direct access to the mean
343 value of the magnetic moment of Fe atoms in Fe-rich nanoparticles (M(0)-Fe-nanop) with no
344 hypothesis.

345 Table 3: Magnetic moment of Fe atoms

SAMPLE	M(0)-nanop (μ_B/atFe-impl)	Fe-nanop	M(0)-Fe-nanop (μ_B)	M(0)-diluted (μ_B/atFe-impl)	Fe_S	M(0)-substit (μ_B)
Sample 1	-	-	-	0.40	-	-
Sample 2	0.5	27	1.85	0.275	53	0.52
Sample 3	0.89	44	2.02	0.10	43	0.23
Sample 4	1.055	-	-	0.11	38	0.29
Sample 5	1.535	66	2.33	0.07	24	0.29
Sample 6	1.285	60	2.14	0.14	35	0.40

Now, taking into account CEMS results, we can also calculate the mean value of the magnetic moment of diluted Fe atoms at the Si sites in the SiC matrix as: M(0)-substit = M(0)-diluted / Fe_S. As shown on Table 3 the median value of M(0)-substit is ~ 0.375 μ_B. Now, we have to remember that there are crystallographic inequivalent Si (and C) sites when the first- and second-nearest neighbours are considered in 6H(4H)-SiC: two (6H-SiC) or one (4H-SiC) with cubic-like symmetry for one with hexagonal-like symmetry [41]. Thus, the mean probability of Fe substitution at an hexagonal-like Si site, which is the only one likely to be magnetic as mentioned above [15], is between 1/3 and ½, and thus the mean value of the magnetic moment of a diluted Fe atom at a hexagonal-like Si site becomes ~ 0.375 x (2 or 3 (~ 2.5)) ~ 0.94 μ_B. In addition, Los *et al* have shown that for such a Fe atom in hexagonal SiC, the energy separation between NM and M is very low (20 meV in 4H-SiC [15]) and M can be FM or antiferromagnetic (AFM) [15-16]. Thus, at a non-zero temperature a diluted Fe atom in a hexagonal-like Si site may be NM, FM or AFM with nearly equal probability (~ 1/3) [15]. The mean value of the magnetic moment of a FM diluted Fe atom is then ~ 0.94 x 3 ~ 2.8 μ_B in very good agreement with the calculated value for such a Fe atom in 2 at%Fe-doped 6H-SiC (2.76 μ_B) [12]. In addition, as shown in [15], depending on the strain state of the crystalline SiC matrix as observed by XRD, the value of the magnetic moment of a FM diluted Fe atom may fluctuate between 2.95 and 3.1 μ_B in 4H-SiC. Such considerations may explain the factor of 2 between the values of experimental magnetization (~ 1.2 μ_B/Mn) [9] and the estimated ones (2.4 μ_B/Mn) [8,9] in (In,Mn)P as suggested by Los et al in [16] for GaN-based DMS materials.

Furthermore, it can be noted that the mean value of the magnetic moment of Fe atoms in the amorphous sample 1 (M(0)-diluted ~ 0.4 μ_B) is almost the same as the median value of M(0)-substit (~ 0.375 μ_B) in crystalline 6H-SiC matrix. We might imagine that each TM atom

in the amorphous SiC is located in elemental thetraedron at a site like a hexagonal Si site in crystalline SiC matrix. In that case Fe_S = 100% for sample 1 and M(0)-substit = M(0)-diluted (~ 0.4 μ_B). This might be suggested by the fact that at the first steps of annealing of an amorphous SiC sample, tiny crystallites of different polytypes are observed [46]. In amorphous SiC, the long range order is broken but short range order may exist and then the discussion of the above paragraph holds and leads to a mean value of the magnetic moment of a FM diluted Fe atom in sample 1 as: 0.4 x 2.5 x 3 ~ 3 μ_B. We can thus conclude that the mean value of the magnetic moment of a FM diluted Fe atom in SiC is ~ 2.8-3.1 μ_B independently of the amorphous or crystalline state of the SiC matrix.

III) Discussion on some typical experimental results

Ferromagnetism with a T_C as high as 250 K has been claimed [18] for Mn- and Fe-implanted 6H-SiC. It can be noted that the temperature dependence of the difference between FC and ZFC magnetization for 5 at.%Fe-implanted 6H-SiC at 623 K and annealed at 973 K (with crystalline SiC matrix and no detected secondary phase) shown in Fig. 3 of [18] has the same behavior as shown in Fig. 6. Following the same normalization procedure as explained above, it appears that we may determine T_C ~ 100-150 K. Experimental results of [18] for the 5 at.%Fe-implanted sample: M(saturation) ~ 0.6 μ_B/atFe and H_C ~ 5 mT at 10 K (Fig. 2 of [18]) and T_C ~ (100-150) K are coherent with those observed in this work. The same behavior is roughly seen on Fig. 4 of [18] for the 5 at.%Mn-implanted sample, with T_C ~ (200 K) and H_C(10 K) ~ 15 mT and about half the magnetization of 5 at.%Fe-implanted sample (Fig.3 of [18]). The discussion of the above paragraph leads to a mean value of the magnetic moment of a FM diluted Mn atom in 5 at.%Mn-implanted SiC as: (0.6 / 2) x 2.5 x 3 ~ 2.25 μ_B in very good agreement with the calculated value for such a Mn atom in 2 at.%Mn-doped 6H-SiC (2.17 μ_B) [12].

Ferromagnetism above RT has also been claimed [47] for 7-10 at.%Cr-doped amorphous SiC films grown on Al_2O_3 substrate with an average magnetic moment in the range 0.17-0.47 μ_B and H_C ~ 3-15 mT between 300 K and 5 K (Fig. 5-6 of [47]). Taking into account the above discussion, we may roughly estimate a mean value of the magnetic moment of FM Cr in SiC as: ((0.17+0.42)/2 = 0.32) x 2.5 x 3 ~ 2.4 μ_B. This value is higher to the values reported for spin moment of a Cr ion in thetrahadral coordination when doped on the Si site (2.0 μ_B) [47], as well as for Cr atom in 2 at%Cr-doped 6H-SiC (1.5 μ_B) [12]. In the corresponding work, there is no correction of the paramagnetic contribution to the SQUID

signal, thus the experimentally estimated values of saturation magnetization are higher than the actual ones. Nevertheless, these values and those of H_C are consistent with those observed for Fe and Mn and we suppose that results described in [47] may be understood in the framework of the theoretical models [8] and [15] as proposed in this work.

From this study and particular examples of refs. [18] and [47], it appears that the FM behavior of diluted TM atoms in SiC does not depend on the crystalline state of the SiC matrix nor on the nature and concentration of the TM dopant in the range of 2-13 at.%, but more on the local relaxation of the SiC lattice due to the substitution of a TM atom at the Si lattice site. The local relaxation may depend on the nature of the TM atom and explain the little differences observed on the values of H_C and T_C and between the calculated and experimentally estimated values of magnetic moments. Moreover, it has been suggested that uniaxial strain as observed in this work can efficiently control the value of T_C resulting from the hole-mediated interaction between magnetic ions in DMS [48]. It would be therefore interesting to perform transport measurements on the Fe-implanted 6H-SiC samples presented in this work in order to study the coupling between magnetic Fe atoms and itinerant carriers. Work is in progress on this topic by our team.

Conclusion

In this paper, we have reviewed some experimental and theoretical results about Fe-(and Mn-Cr-) implanted SiC. We have shown that Fe:SiC has similar electronic structure and magnetic behavior to (In,Mn)P. Combining many selected experimental techniques and properly treating magnetometry results together with the help of new theoretical approaches adapted to the studied system allow a direct access to:

1- The mean value of the magnetic moment of Fe atoms in magnetic Fe-rich nanoparticles (~ 2.1 μ_B) currently observed for Fe atoms in the high spin state in well defined solid FM compounds mainly detected in the core of the Fe-rich nanoparticles.
2- The mean value of the magnetic moment of FM diluted Fe atoms (~ 2.8 μ_B) (2.2 μ_B for Mn) in very good agreement with the calculated value for such TM atoms in hexagonal SiC. This value together with the temperature dependence of their magnetization strongly agree with recent theoretical works on such DMS systems taking into account both the carrier-mediated ferromagnetism and the correct location of the transition metal dopant binding energy in the host semiconductor, allowing us to

conclude that FM diluted Fe atoms in 2-13 at.%Fe-implanted SiC have a DMS behavior.

The magnetic moment of FM diluted Fe atoms in SiC appears due to local strain relaxation around the implanted species. It is also independent of the amorphous or crystalline state of the SiC matrix and of the presence of small (diameter < 10 nm) superparamagnetic Fe-rich nanoparticles. However, the value of their T_C is strongly dependent on the presence of larger (diameter > 10 nm) FM Fe-rich nanoparticles, decreasing from ~ 115 K to 45 K in presence of Fe_3Si nanoparticles. This experimental work may contribute to a better understanding of the complex topic of the effects of nanometric magnetic inhomogeneities of diluted magnetic systems.

Acknowledgements

A.M. Archambaud (1), for samples preparation; M. Marteau (1) for ion implantations; D. Eyidi (1) for TEM, SEM and EDS measurements; M. Viret (CEA/SPEC-Saclay) for magnetometric measurements; A. Debelle (CSNSM-Orsay) for RBS checking of the samples; Region of Normandy and the European Regional Development Fund of Normandy (ERDF) in the frame of the MAGMA project funded this work.

References

[1] I. Žutić, J. Fabian, and S. Das Sarma, Rev. Mod. Phys. 76, 323 (2004).

[2] J. Cibert and D. Ferrand, Journal du CNRS (2003-2004) p. 99.

[3] A. Bonanni, T. Dietl, Chem. Soc. Rev. 39, 528 (2010).

[4] H. Shinya, T. Fikishima, A. Masago, K. Sato, and H. Katayama-Yoshida, Phys. Rev. B 96, 104415 (2017).

[5] T. Dietl, H. Ohno and F. Matsukurz, Phys. Rev. B 63,1 (2001).

[6] K. Sato, L. Bergqvist, J. Kudrnovský, P. H. Dederichs, O. Eriksson, I. Turek, B. Sanyal, G. Bouzerar, H. Katayama-Yoshida, V. A. Dinh, T. Fukushima, H. Kizaki, R. Zeller, Rev. Mod. Phys. 82, 1633 (2010).

[7] G. Bouzerar and R. Bouzerar, Comptes Rendus Physique 16, 731 (2015).

[8] R. Bouzerar, D. May, U. Löw, D. Machon, P. Melinon, S. Zhou, and G. Bouzerar, Phys. Rev. B 94, 094437 (2016).

[9] M. Khalid, E. Weschke, W. Skorupa, M. Helm, and S. Zhou,, Phys. Rev. B 89, 121301(R) (2014).

[10] A. Chakraborty, P. Wenk, S. Kettemann, R. Bouzerar, and G. Bouzerar, New J. of Physics 16, 033004 (2014).

[11] Woodhead Publishing Series in Electronic and Optical Materials: Number 87, Edited by V. Dierolf, I.T. Ferguson, J.M. Zavada (2016).

[12] V.L. Shaposhnikov and N.A. Sobolev, Journal of Physics: Condensed Matter 16, 1761 (2004).

[13] M.S. Miao. and W.R.L. Lambrecht, Physical Review B 68, 125204 (2003).

[14] M.S. Miao. and W.R.L. Lambrecht, Physical Review B 74, 235218 (2006).

[15] A.V. Los, A.N. Timoshevskii, V.F. Los, and S.A. Kalkuta, Physical Review B 76, 165204 (2007).
[16] A. Los, and V. Los, Journal of Physics: Condensed Matter 21, 206004 (2009).
[17] A.V. Los and V. Los, J. Phys. Condens. Mater. 22, 245801 (2010).
[18] N. Theodoropoulou, A.F. Hebard, S.N.G. Chu, M.E. Overberg, C.R. Abernathy, S.J. Pearton, R.G. Wilson, and J.M. Zavada, Electrochemical and Solid-State Letters 4, G119 (2001).
[19] B. Song, H. Bao, H. Li, M. Lei, J. Jian, J. Han, X. Zhang, S. Meng, W. Wang, and X. Chen, Applied Physics Letters 94, 102508 (2009).
[20] Y. Liu, G. Wang, S. Wang, J. Yang, L. Chen, X. Qin, B. Song, B. Wang, and X. Chen, Physical Review Letters 106, 087205 (2011).
[21] F. Stromberg, W. Keune, X. Chen, S. Bedenta, H. Reuter, and A. Mücklich, J. Phys.: Condens. Matter 18, 9881 (2006).
[22] A. Declémy, M. Drouet, J.P. Eymery, C. Dupeyrat, F. Ott, and M. Viret, Phys. Status Solidi C 4, 1473 (2007).
[23] M.L. Diallo, A. Fnidiki, M. Viret, M. Drouet, D. Eyidi, and A. Declémy, Phys. Status Solidi C 12, 60 (2015).
[24] M.L. Diallo, L. Lechevallier, A. Fnidiki, R. Lardé, A. Debelle, L. Thomé, M. Viret, M. Marteau, D. Eyidi, A. Declémy, F. Cuvilly, and I. Blum, J. App. Phys. 117, 183907 (2015).
[25] B. Song, J.K. Jian, H. Li, M. Lei, H.Q. Bao, X.L. Chen, and G. Wang, Physica B: Condensed Matter 403, 2897 (2008).
[26] L. Diallo, A. Fnidiki, L. Lechevallier, A. Zarefy, J. Juraszek, F. Cuvilly, I. Blum, M. Viret, M. Marteau, D. Eyidi, and A. Declémy, IEEE Magnetics Letters 9, 1-3 (2018).
[27] L. Zhang, L. Diallo, A. Fnidiki, L. Lechevallier, A. Declémy, W. Lefebvre, J. Juraszek, Scripta Materialia 188, 157 (2020).
[28] M.L. Diallo, L. Diallo, A. Fnidiki, L. Lechevallier, F. Cuvilly, I. Blum, M. Viret, M. Marteau, D. Eyidi, J. Juraszek, and A. Declémy, Journal of Applied Physics 122, 083905 (2017).
[29] L. Diallo, A. Fnidiki, L. Lechevallier, J. Juraszek, M. Viret, M. Marteau, D. Eyidi, and A. Declémy, Journal of Applied Physics 127, 183901 (2020).
[30] W.J. Weber, L.M. Wang, N. Yu, and N.J. Hess, Materials Science and Engineering. A. Structural Materials: Properties, Microstructure and Processing 253, 62 (1998).
[31] A. Declémy, A. Debelle, C. Dupeyrat, L. Thomé, I. Monnet and D. Eyidi, Applied Physics A 106, 679 (2012).

509 [32] B. Gault, F. Vurpillot, A. Vella, M. Gilbert, A. Menand, D. Blavette, and B. Deconihout,
510 Review of Scientific Instruments 77, 043705 (2006).
511 [33] N. Sousbie, L. Capello, J. Eymery and F. Rieutord, C. Lagahe, Journal of Applied
512 Physics 99, 103509 (2006).
513 [34] S. Stepanov, GID-sl. https://x-server.gmca.aps.anl.gov/GID_sl.html.
514 [35] S. Leclerc, M.F. Beaufort, A. Declémy, J.F. Barbot, Journal of Nuclear Materials 397,
515 132 (2010).
516 [36] J.F. Barbot, S. Leclerc, C. Tromas, V. Audurier, A. Declémy, M. Texier, M-F. Beaufort,
517 Materiels Science Forum 717-720, 485 (2012).
518 [37] A. Fnidiki, F. Richomme, J. Teillet, F. Pierre, P. Boher, Ph. Houdy, J. Magn. Magn. Mat.
519 121, 520 (1993).
520 [38] J. Juraszek, O. Zivotsky, H. Chiron, C. Vaudolon and J. Teillet, Rev. Sci. Instrum., 80
521 043905 (2009).
522 [39] H.P.Gunnlaugsson, K. Bharuth-Ram, M. Dietrich, M. Fanciulli, H.O.U. Fynbo, and G.
523 Weyer, Hyper. Interact. 169, 1319 (2006).
524 [40] V.A. Gubanov, C. Boekema, and C.Y. Fong, Appl. Phys. Lett. 78, 216 (2001).
525 [41] K. Racka, A. Avdonin, M. Sochacki, E. Tymicki, K. Grasza, R. Jakiela, B. Surma, W.
526 Dobrowolski, Journal of Crystal Growth 413, 86 (2015).
527 [42] T. Sahu, Physical Letters A 115,173 (1986).
528 [43] Y. Wang, Dissertation “Defect-induced ferromagnetism in SiC”, Institut für
529 Ionenstrahlphysik und Materialforschung, Helmholtz-Zentrum, Dresden-Rossendorf,
530 (15.10.2014/30.01.2015) p.39.
531 [44] G. Herzer, IEEE Transactions on Magnetics 25, 3327 (1989).
532 [45] A. Ślawska-Waniewska, M. Gutowski, and H.K. Lachowicz, Physical Review B 46,
533 14594 (1992).
534 [46] E. Oliviero, M. L. David, and M. F. Beaufort, J. Nomgaudyte and L. Pranevicius, A.
535 Declémy and J. F. Barbot, Journal of Applied Physics 91, 1179 (2002).
536 [47] C. Jin, L. Zhuge, Z. Sha, B. Hong, J. Phys. D: Appl. Phys. 41, 035005 (2008).
537 [48] Y. Semenov, V. Stephanovich, Physical Review B 67, 195203 (2003).
538 [49] J.F. Barbot, M.F. Beaufort, M. Texier, C. Tromas, J. Nucl. Mater. 413, 162 (2011).
539 [50] J.F. Ziegler, http://www.srim.org/
540 [51] F. Zhang and A.R. Oganov, Geophysical Resaerch Letters 37, L02305 (2010).
541 [52] Y. Katoh, N. Hashimoto, S. Kondo, L.L. Snead, A. Kohyama, J. Nucl. Mater. 351, 228
542 (2006).

Fe-doped SiC

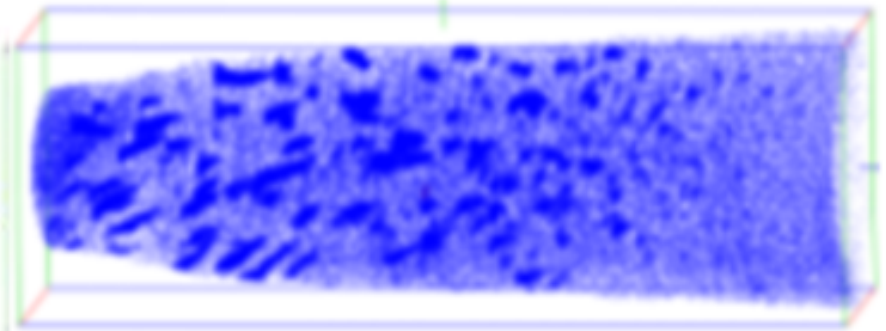

Fe atoms

$41.4 \times 41.5 \times 132.5\ nm^3$